Vehicle System Dynamics
International Journal of Vehicle Mechanics and Mobility

ISSN: 0042-3114 (Print) 1744-5159 (Online) Journal homepage: http://www.tandfonline.com/loi/nvsd20

The effect of wheel set gyroscopic action on the hunting stability of high-speed trains

Xiao-Hui Zeng, Han Wu, Jiang Lai & Yang Yu

To cite this article: Xiao-Hui Zeng, Han Wu, Jiang Lai & Yang Yu (2017) The effect of wheel set gyroscopic action on the hunting stability of high-speed trains, Vehicle System Dynamics, 55:6, 924-944, DOI: 10.1080/00423114.2017.1293833

To link to this article: http://dx.doi.org/10.1080/00423114.2017.1293833

VEHICLE SYSTEM DYNAMICS, 2017
VOL. 55, NO. 6, 924–944
http://dx.doi.org/10.1080/00423114.2017.1293833

IAVSD
Taylor & Francis
Taylor & Francis Group

The effect of wheel set gyroscopic action on the hunting stability of high-speed trains

Xiao-Hui Zeng[a,b], Han Wu[a,b], Jiang Lai[c] and Yang Yu[d]

[a]Key Laboratory for Mechanics in Fluid Solid Coupling Systems, Institute of Mechanics, Chinese Academy of Sciences, Beijing, People's Republic of China; [b]School of Engineering Science, University of Chinese Academy of Sciences, Beijing, People's Republic of China; [c]Nuclear Power Institute of China, Chengdu, People's Republic of China; [d]State Key Laboratory of Hydraulic Engineering Simulation and Safety, School of Civil Engineering, Tianjin University, Tianjin, People's Republic of China

ABSTRACT

This study explores the effects of wheel set gyroscopic action on hunting stability by calculating linear and nonlinear critical speeds. First, a dynamic model for a high-speed vehicle with 23 degrees of freedom is developed by considering wheel set gyroscopic action. The linear and nonlinear critical speeds are calculated by eigenvalue analysis and drawing a bifurcation map, respectively. Two computer programs for linear and nonlinear stability analysis are developed. Second, based on an actual high-speed vehicle in China, the effects of wheel set gyroscopic action on hunting stability are quantitatively investigated using computer simulation. Furthermore, the difference between the effects of gyroscopic moments about the *x*-axis and *z*-axis is discussed. The results show that the moment about the *x*-axis is harmful to hunting stability, but the moment about the *z*-axis is beneficial to hunting stability. However, the integrated effect of these two moments can enhance the critical speeds and suppress the hunting motion.

ARTICLE HISTORY
Received 10 May 2016
Revised 30 January 2017
Accepted 5 February 2017

KEYWORDS
Wheel set gyroscopic action; hunting stability; critical speed

1. Introduction

Currently, the running speed of high-speed rail in China is about 300 km/h, and it will probably exceed 400 km/h in the future. When the train is running at high speeds, there are new safety challenges. The hunting stability is an important index of safety for railway vehicles. Regarding hunting stability, certain factors that can be ignored at low speeds become very important at high speeds, and wheel set gyroscopic action is the most representative among them. At a running speed of 300 km/h, the rotational frequency of the wheel set reaches 30 r/s, and the angular velocity can reach 83 rad/s. If the wheel set incurs roll and yaw motion in this condition, the wheel set gyroscopic action will be fairly obvious.

Extensive investigations in linear and nonlinear hunting stability of railway vehicles on straight and curved tracks have been reported. Kim et al. [1], Lee and Cheng [2,3], Cheng and Lee [4], Cheng [5] and Cheng and Hsu [6] study the linear stability characteristics of railway vehicles using the eigenvalue analysis, and analyse the influence of suspension

CONTACT Han Wu wuhan@imech.ac.cn

parameters and creep models on linear critical speed. Allen and Iwnicki [7] compare the critical speeds of vehicles on a track and on a roller rig. True [8] defines the nonlinear critical speed in such a way that it is theoretically guaranteed that no hunting motion can take place at speeds below the critical speed. He hypothesises that the nonlinear critical speed should be taken as the criterion for the speed limit. True [9,10] and True and Kaas-Petersen [11] describe the basic theory of bifurcation analysis of nonlinear vehicle systems, and show that the correct approach for determining the nonlinear critical speed is to find the smallest bifurcation point using the path-following method. Kim and Seok [12] perform a bifurcation analysis on a nonlinear railway vehicle with dual bogies to examine the coupling effect of the bogies on the vehicle's hunting behaviour. Polach and Kaiser [13] analyse the hunting behaviour of a vehicle system using two different methods: a path-following method and a brute-force method. The results using these two methods are compared. True [14], Jensen and True [15] and True and Jensen [16] study chaos and asymmetry hunting on railway vehicle dynamics, present bifurcation diagrams, and investigate the dynamics of bogie models with realistic wheel and rail profiles. Sedighi and Shirazi [17] present 2-D and 3-D bifurcation diagrams, and investigate the effect of suspension parameters, wheel set mass, and wheel conicity on critical speed. Eom et al. [18] carry out theoretical analysis and experimental study using a small-scale bogie model. Dong et al. [19] obtain the bifurcation diagrams of a vehicle system by the shooting method, and perform an extensive analysis on bifurcation characteristics of the CRH vehicles. Huang et al. [20] study low-frequency hunting motion of high-speed vehicles by numerical simulation and field experimentation, and the results regarding the influence of suspension parameters are provided. Zeng et al. [21,22] investigate the influence of aerodynamic loads on hunting stability of high-speed vehicles. Zboinski and Dusza [23–26] conduct numerous of studies on the nonlinear stability of railway vehicles running on a curved track by drawing bifurcation diagrams. The studies involve the influence of suspension parameters, rail radius and inclination, and wheel–rail profile and mean rolling radius on the hunting stability. Zeng and Wu [27] study the critical speed at the Hopf bifurcation point on a circular curved track. The influences of track curve radius and super elevation on nonlinear critical speed are investigated.

The wheel set gyroscopic action is a significant factor that influences the hunting stability of high-speed railway vehicles. There are few studies on the effect of wheel set gyroscopic action on hunting stability. Hirotsu [28] calculates the change of hunting motion after considering wheel set gyroscopic action. According to Hirotsu's research, the vehicle vibration becomes weak because of wheel set gyroscopic action. He qualitatively indicates that the wheel set gyroscopic action is beneficial for hunting stability. Based on the research regarding the stability of cone tread wheel sets, Huang [29] obtains the contribution rate of wheel set gyroscopic moment by matrix operations. He analyses the influence of vehicle speed, equivalent conicity, and primary stiffness on the contribution rate. He concludes that gyroscopic action is induced by the spin creep coefficient and pitch moment of inertia, and that the contribution rate increases with increasing vehicle speed.

The above research provides a certain understanding of the wheel set gyroscopic effect, and provides references for us. However, there are three points about the current research that require explanation. First, the above research is limited to qualitative research; the influence of wheel set gyroscopic action on critical speed has not been studied. Second, Huang's research [29] is conducted for cone tread wheel set and linear stability, and is

much different from the situation of the whole vehicle. Third, it is known that the wheel set gyroscopic action behaves as the moments about the x-axis and z-axis. The difference between these two moments is the focus of our research.

In consideration of these points, the effect of wheel set gyroscopic action on hunting stability should be quantitatively analysed in detail. In order to conduct this study, a dynamic model of high-speed vehicles considering wheel set gyroscopic action is developed. The mechanics of the effect of wheel set gyroscopic action on hunting stability is discussed on the basis of the governing equations. On the basis of previous [21,22] studies, we develop computational programs to analyse the effect of wheel set gyroscopic action. We calculate the influence of wheel set gyroscopic action on the characteristics of hunting stability, such as linear critical speed, nonlinear critical speed, bifurcation diagrams, and amplitude of hunting motion.

This paper is structured as follows. In Section 2, we introduce the vehicle dynamical system and the method of stability analysis. Section 3 describes the effect of wheel set gyroscopic action on linear stability. Section 4 describes the effect on nonlinear stability. The two aspects of effects on yaw motion and normal contact force, namely the influences of the moment about the z-axis and the moment about the x-axis, are compared in Section 5. Finally, the conclusions are presented in Section 6.

2. Model and theory

2.1. Vehicle dynamical model

To quantitatively study the effects of gyroscopic action on hunting stability, a dynamical model of a high-speed railway vehicle is developed, referring to an actual high-speed railway vehicle that is widely used in China. Figure 1 is a sketch of the railway vehicle

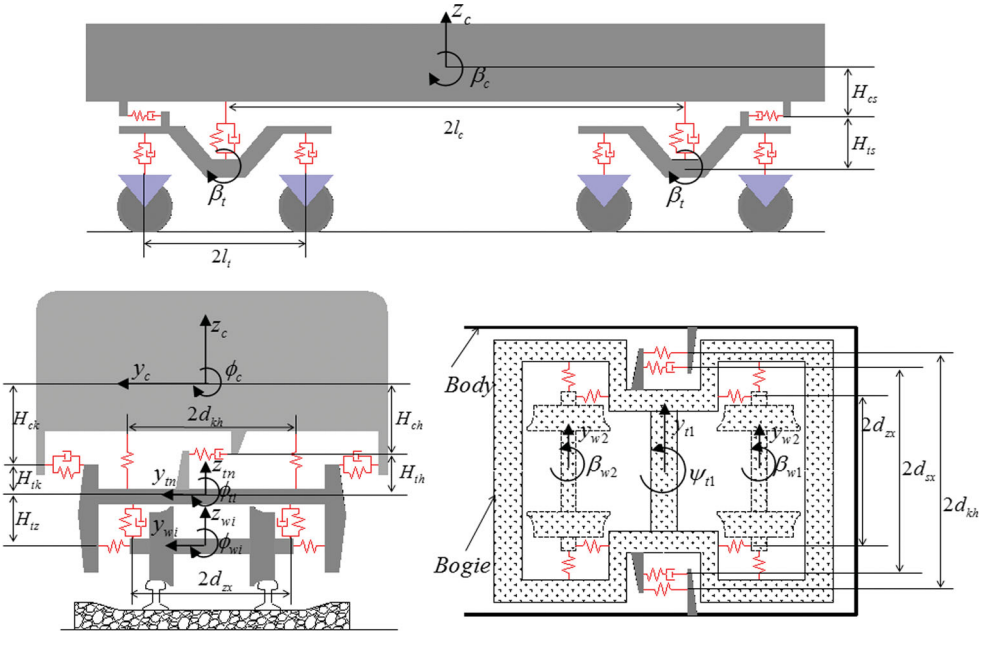

Figure 1. A sketch of the railway vehicle dynamical system [22].

Table 1. DOF of the vehicle.

	Motion				
Vehicle Parts	Lateral	Vertical	Roll	Yaw	Pitch
Body	y_c	z_c	ϕ_c	ψ_c	β_c
Bogies ($n = 1,2$)	y_{tn}	z_{tn}	ϕ_{tn}	ψ_{tn}	β_{tn}
Wheel sets ($i = 1-4$)	y_{wi}			ψ_{wi}	

dynamical system [22]. The dynamical model contains 23 degrees of freedom (DOF). Table 1 shows the 23 DOFs.

The wheel set roll angle ϕ_w and the vertical displacement z_w are not independent variables, but are subject to wheel/rail geometric constraints and lateral motion of the wheel set. The wheel/rail profile LMA/UIC60 is adopted in this study.

In this study, both lateral dampers and the yaw dampers are modelled by the connection of spring and damping in series. We consider the lateral displacements of the spring–damping connecting point of the lateral dampers $y_{hi}(i = 1,\ 2)$, and the longitudinal displacements of the spring–damping connecting point of four yaw dampers y_{sLi} and $y_{sRi}(i = 1,\ 2)$. There are six DOFs of the connecting points.

Consider a railway vehicle moving on a flat and straight track. The governing differential equations for motion of the vehicle are given as Equations (1)–(14).

For the wheel sets,

$$\begin{aligned} &m_w\ddot{y}_{wi} - 2k_{py}[-y_{wi} + y_{tn} + h_{tz}\phi_{tn} - (-1)^i l_t\psi_{tn}] \\ &\quad = -N_{Li}\sin(\lambda_{ri} + \phi_{wi}) + N_{Ri}\sin(\lambda_{li} - \phi_{wi}) + F_{yLi} + F_{yRi}, \end{aligned} \tag{1}$$

$$\begin{aligned} &I_{wz}\ddot{\psi}_{wi} + I_{wy}\frac{V}{R_0}\dot{\phi}_w + 2d_{zx}k_{px}(d_{zx}\psi_{wi} - d_{zx}\psi_{tn}) \\ &\quad = d_0(F_{xRi} - F_{xLi}) + d_0\psi_{wi}(F_{yRi} - F_{yLi}) \\ &\qquad + M_{zi} + d_0\psi_{wi}[N_{Ri}\sin(\lambda_{ri} - \phi_{wi}) + N_{Li}\sin(\lambda_{li} + \phi_{wi})]\cos\psi_{wi}, \end{aligned} \tag{2}$$

where $n = 1$ for $i = 1, 2$ and $n = 2$ for $i = 3, 4$. It is noted that in Equations (1) and (2), the subscript $n = 1$ or 2 denote the front and the rear frame, and the subscript $i = 1$–4 denote the ith wheel set, respectively. The wheel set roll angle ϕ_w and the vertical displacement z_w are not independent variables, but subject to wheel/rail geometric constraints and lateral motion of the wheel set. Hence, there are no independent equations with respect to roll motion and vertical motion similar to the equations of lateral motion and yaw motion given by Equations (1) and (2).

For the bogies,

$$\begin{aligned} &m_t\ddot{y}_{ti} + 2k_{py}(2y_{ti} - y_{w(2i)} - y_{w(2i-1)} + 2h_{tz}\phi_{ti}) \\ &\quad - 2k_{ty1}(-y_{ti} + y_c + h_{tk}\phi_{ti} + h_{ck}\phi_c - (-1)^i l_c\psi_c) \\ &\quad - k_{ty2}(y_{hi} - y_{ti} + h_{th}\phi_{ti}) = 0, \end{aligned} \tag{3}$$

$$\begin{aligned} &m_t\ddot{z}_{ti} + 2k_{pz}(2z_{ti} - z_{w(2i)} - z_{w(2i-1)}) + 2c_{pz}(2\dot{z}_{ti} - \dot{z}_{w(2i)} - \dot{z}_{w(2i-1)}) \\ &\quad - 2k_{tz1}[z_c - z_{ti} + (-1)^i l_c\beta_c] = 0, \end{aligned} \tag{4}$$

$$I_{tx}\ddot{\phi}_{ti} + 2k_{py}h_{tz}(y_{w(2i-1)} + y_{w(2i)} - 2y_{ti} - 2h_{tz}\phi_{ti}) + 2k_{pz}d_{zx}^2(2\phi_{ti} - \phi_{w(2i-1)} - \phi_{w2i}) + 2c_{pz}d_{zx}^2(2\dot{\phi}_{ti} - \dot{\phi}_{w(2i-1)} - \dot{\phi}_{w2i}) - 2h_{tk}k_{ty1}[y_{ti} - y_c - h_{tk}\phi_{ti} - h_{ck}\phi_c + (-1)^i l_c\psi_c] + h_{th}k_{ty2}(y_{hi} - y_{ti} + h_{th}\phi_{ti}) + 2d_{kh}^2k_{tz1}(\phi_{ti} - \phi_c) = 0, \quad (5)$$

$$I_{tz}\ddot{\psi}_{ti} - 2k_{py}l_t(y_{w(2i-1)} - y_{w(2i)} - 2l_t\psi_{ti}) - 2k_{px}d_{zx}^2(\psi_{w(2i-1)} + \psi_{w(2i)} - 2\psi_{ti}) - 2d_{kh}^2k_{tx1}(\psi_c - \psi_{ti}) - d_{sx}k_{sx}(y_{sRi} - y_{sLi} - 2d_{sx}\psi_{ti}) = 0, \quad (6)$$

$$I_{ty}\ddot{\beta}_{ti} - 2l_tk_{pz}(-z_{w(2i-1)} + z_{w(2i)} - 2l_t\beta_{ti}) - 2l_tc_{pz}(-\dot{z}_{w(2i-1)} + \dot{z}_{w(2i)} - 2l_t\dot{\beta}_{ti}) + 4h_{tz}^2k_{px1}\beta_{ti} + h_{ts}k_{sx}(2h_{ts}\beta_{ti} + y_{sLi} + y_{sRi}) + 2h_{tk}k_{tx1}(h_{ck}\beta_c + h_{tk}\beta_{ti}) = 0, \quad (7)$$

where $i = 1, 2$. The subscripts $i = 1$ and 2 in Equations (3)–(7) denote the front and the rear frame, respectively.

For the car body:

$$m_c\ddot{y}_c - 2k_{ty1}(y_{t1} + y_{t2} - 2y_c - h_{tk}\phi_{t1} - h_{tk}\phi_{t2} - 2h_{ck}\phi_c) + k_{ty2}(-y_{t1} + h_{th}\phi_{t1} + y_{h1}) + k_{ty2}(-y_{t2} + h_{th}\phi_{t2} + y_{h2}) = F_{y\_wind}, \quad (8)$$

$$m_c\ddot{z}_c + 2k_{tz1}(2z_c - z_{t1} - z_{t2}) = F_{z\_wind}, \quad (9)$$

$$I_{cx}\ddot{\phi}_c - 2k_{ty1}h_{ck}(y_{t1} + y_{t2} - 2y_c - h_{tk}\phi_{t1} - h_{tk}\phi_{t2} - 2h_{ck}\phi_c) + h_{ch}k_{ty2}(-y_{t1} + h_{th}\phi_{t1} + y_{h1}) + h_{ch}k_{ty2}(-y_{t2} + h_{th}\phi_{t2} + y_{h2}) - 2k_{tz1}d_{kh}^2(\phi_{t1} + \phi_{t2} - 2\phi_c) = M_{x\_wind}, \quad (10)$$

$$I_{cz}\ddot{\psi}_c - 2k_{ty1}l_c(y_{t1} - y_{t2} - h_{tk}\phi_{t1} + h_{tk}\phi_{t2} - 2l_c\psi_c) + l_ck_{ty2}(-y_{t1} + h_{th}\phi_{t1} + y_{h1}) - l_ck_{ty2}(-y_{t2} + h_{th}\phi_{t2} + y_{h2}) + d_{sx}k_{sx}(-2d_{sx}\psi_{t1} + y_{sR1} - y_{sR1}) + d_{sx}k_{sx}(-2d_{sx}\psi_{t2} + y_{sR2} - y_{sL2}) - 2k_{tx1}d_{kh}^2(\psi_{t1} + \psi_{t2} - 2\psi_c) = M_{z\_wind}, \quad (11)$$

$$I_{cy}\ddot{\beta}_c - 2k_{tz1}l_c(z_{t2} - z_{t1} - 2l_c\beta_c) + 2k_{tx1}h_{ck}(2h_{ck}\beta_c + h_{tk}\beta_{t1} + h_{tk}\beta_{t2}) - h_{cs}k_{sx}(2h_{ts}\beta_{t1} + y_{sL1} + y_{sR1}) - h_{cs}k_{sx}(2h_{ts}\beta_{t2} + y_{sL2} + y_{sR2}) = M_{y\_wind}. \quad (12)$$

For the connecting point of lateral dampers and yaw dampers,

$$k_{ty2}(y_{ti} - h_{th}\phi_{ti} - y_{hi}) - c_{ty2}[\dot{y}_{hi} - \dot{y}_c - h_{ck}\dot{\phi}_c + (-1)^i l_c\dot{\psi}_c] = 0, \quad (13)$$

$$k_{sx}(h_{ts}\beta_{ti} + y_{sLi} + d_{sx}\psi_{ti}) + c_{sx}(h_{cs}\dot{\beta}_c + d_{sx}\dot{\psi}_c + \dot{y}_{sLi}) = 0,$$

$$k_{sx}(h_{ts}\beta_{ti} + y_{sRi} - d_{sx}\psi_{ti}) + c_{sx}(h_{cs}\dot{\beta}_c - d_{sx}\dot{\psi}_c + \dot{y}_{sRi}) = 0. \quad (14)$$

where $i = 1$ and 2 denote the dampers on the front and on the rear frame, respectively. All the physical quantities in Equations (1)–(14) are defined in Appendix 1. The nominal design parameters of the vehicle system are provided in Appendix 2. F_{y_wind}, F_{z_wind}, M_{x_wind}, M_{z_wind}, and M_{y_wind} are the components of aerodynamic loads. The interest in this study is on the analysis of the effect of wheel set gyroscopic action on hunting stability of a railway vehicle on a straight track, so they are set to zero.

2.2. Normal contact force and creep force

The nonlinear wheel/rail relationship is the most important nonlinear factor in the dynamical system of a railway vehicle. In this study, the LMA/UIC60 wheel/rail profile is adopted. The profile of a wheel/rail includes several curves, and the wheel/rail contact relationship includes wheel set rolling radius, contact angle, roll angle of the wheel set, transverse radius of wheel profile, and transverse radius of rail profile. The wheel/rail contact relationship can be considered as nonlinear functions of wheel set lateral displacement y_w. Because of the difficulty of expressing those contact parameters as explicit functions of y_w, the profiles of wheel and rail are described as a discrete point set in terms of y_w. The contact parameters are calculated by using spline interpolation. The wheel/rail normal contact forces and creep forces can then be calculated by the obtained contact parameters.

The normal contact forces can be obtained by the motion equations of roll angle ϕ_w and vertical displacement z_w of the wheel set (ϕ_w and z_w are subject to wheel/rail geometric constraints, not independent), as shown in Equation (15). F_{pzL} and F_{pzR} are the change of the stiffness force of primary suspension f_{pzL} and f_{pzR} are the change of the damping force of primary suspension. The others are defined in Appendix 1.

$$\begin{aligned} N_L &= 2\cos(\lambda_L+\phi_w)(W+M_w\ddot{z}_w-F_{pzL}-F_{pzR}-f_{pzL}-f_{pzR}) \\ &\quad+\frac{2\cos(\lambda_L+\phi_w)}{d_0}\begin{pmatrix}-\boldsymbol{I_{wy}}\dfrac{\boldsymbol{V}}{\boldsymbol{R_0}}\dot{\boldsymbol{\psi}}_{\boldsymbol{w}}-d_{zx}F_{pzL}+d_{zx}F_{pzR}-d_{zx}f_{pzL}+d_{zx}f_{pzR}\\ -F_{yL}R_L-F_{yR}R_R-R_RN_R\sin(\lambda_R-\phi_w)+R_LN_L\sin(\lambda_L+\phi_w)\end{pmatrix} \\ N_R &= 2\cos(\lambda_R-\phi_w)(W+M_w\ddot{z}_w-F_{pzL}-F_{pzR}-f_{pzL}-f_{pzR}) \\ &\quad-\frac{2\cos(\lambda_R-\phi_w)}{d_0}\begin{pmatrix}-\boldsymbol{I_{wy}}\dfrac{\boldsymbol{V}}{\boldsymbol{R_0}}\dot{\boldsymbol{\psi}}_{\boldsymbol{w}}-d_{zx}F_{pzL}+d_{zx}F_{pzR}-d_{zx}f_{pzL}+d_{zx}f_{pzR}\\ -F_{yL}R_L-F_{yR}R_R-R_RN_R\sin(\lambda_R-\phi_w)+R_LN_L\sin(\lambda_L+\phi_w)\end{pmatrix}. \end{aligned} \tag{15}$$

According to Kalker's linear creep theory [30], the creep forces and moments are calculated by Equation (16), where F_x is the longitudinal creep force and F_y is the lateral creep force. The terms γ_x, γ_y, and γ_s are the longitudinal, lateral and spin creepages, respectively.

$$\begin{aligned} F_x &= -f_{11}\gamma_x, \\ F_y &= -f_{22}\gamma_y - f_{23}\gamma_s, \\ M_z &= f_{23}\gamma_y - f_{33}\gamma_s. \end{aligned} \tag{16}$$

The creep coefficients are calculated as follows:

$$\begin{aligned} f_{11} &= G(ab)C_{11}, \\ f_{22} &= G(ab)C_{22}, \\ f_{23} &= G(ab)^{3/2}C_{23}, \\ f_{33} &= G(ab)^2C_{33}, \end{aligned} \tag{17}$$

where G is the combined modulus of rigidity, a and b represent the contact ellipse semi-axes, and C_{11}, C_{22}, C_{23}, and C_{33} are the coefficients that have been tabulated in Ref. [31].

In order to evaluate the wheel/rail creep forces more accurately, Shen–Hedrick–Elkins' nonlinear creep force model [32] is used:

$$F = \sqrt{F_x^2 + F_y^2}, \tag{18}$$

$$F' = \begin{cases} f \cdot N \left[\dfrac{F}{f \cdot N} - \dfrac{1}{3}\left(\dfrac{F}{f \cdot N}\right)^2 + \dfrac{1}{27}\left(\dfrac{F}{f \cdot N}\right)^3 \right] & (F \le 3fN), \\ f \cdot N & (F > 3fN), \end{cases} \tag{19}$$

where f is the friction coefficient. Saturation constant ε is calculated by Equation (20).

$$\varepsilon = \frac{F'}{F}. \tag{20}$$

The modified creep forces and moments are obtained as

$$\begin{aligned} F'_x &= \varepsilon \cdot F_x, \\ F'_y &= \varepsilon \cdot F_y, \\ M'_z &= \varepsilon \cdot M_z. \end{aligned} \tag{21}$$

2.3. Method of analysis of linear and nonlinear stability

To investigate the effect of wheel set gyroscopic action on linear stability, we linearise the nonlinear dynamic equations of the vehicle system at the centre of the track. The governing differential equations for the motion of the vehicle can be re-expressed by the following system of first-order differential equations [33]:

$$\dot{\mathbf{x}} = \mathbf{f}[x(t)]. \tag{22}$$

For any given vehicle speed, the following matrix can be defined:

$$\mathbf{A} = \left(\frac{\partial \mathbf{f}}{\partial \mathbf{x}}\right)\Bigg|_{\mathbf{x}=\mathbf{0}}. \tag{23}$$

The stability of the nonlinear system described by Equation (22) in the neighbourhood of its equilibrium point can be determined by the eigenvalues of matrix **A**. If all the eigenvalues have negative real parts, the system is asymptotically stable. If there is at least one eigenvalue with a positive real part, the system is unstable. When the maximum real part turns out to be zero, the vehicle system reaches a critical state, and the corresponding speed is the critical speed of hunting stability. A computer program capable of incorporating the effects of wheel set gyroscopic action is developed.

As for the dynamical system of a railway vehicle with subcritical bifurcation, the nonlinear critical speed should be the smallest bifurcation point [9]. An appropriate way to determine the smallest bifurcation point is to apply the method known as path following. In order to calculate the nonlinear critical speed, the governing differential equations are solved by the Runge–Kutta method, and a computer program capable of calculating the response of the nonlinear vehicle dynamical system is developed. According to

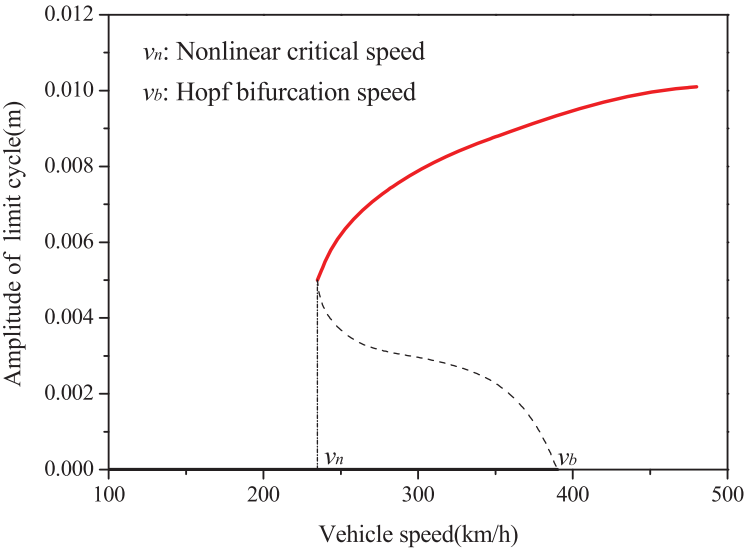

Figure 2. A schematic diagram of nonlinear critical speed [22].

True's method, we change the vehicle speed manually in small steps and solve the initial-value problem for obtaining the dynamic response in each step. In each step, the solution of the previous step is taken as the initial condition. When the solution of the previous step is stationary, the speed is increased in the next step, and the initial condition of the subsequent calculation is given by a small disturbance ($y_{w1} = 0.5$ mm in this study). The speed where the nonlinear system tends to a periodic solution is called the Hopf bifurcation speed v_b, as shown in Figure 2. The speed is increased continually until the amplitude of the periodic solution becomes quite large. Then, we begin to decrease the vehicle speed. The solution of a periodic solution for a slightly greater vehicle speed is taken as the initial condition for subsequent calculation. At a certain speed, the initial-value problem of the nonlinear system tends to a stable zero solution. This speed is the smallest bifurcation point, which corresponds to the nonlinear critical speed v_n, as shown in Figure 2 [22].

2.4. Gyroscopic action of wheel set

A schematic diagram of wheel set motion is presented in Figure 3. The positive direction of the x-axis is the heading direction of the vehicle. The yaw motion and roll motion of

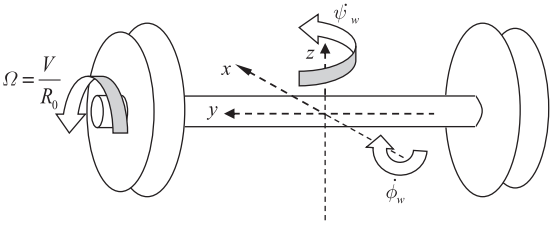

Figure 3. A schematic diagram of wheel set motion.

the wheel set can result in obvious gyroscopic action when the train is running at a high speed. The gyroscopic action behaves as two moments – the moment about the x-axis and the moment about the z-axis. As shown in Equations (24) and (25), the value of the gyroscopic moment of a wheel set is proportional to vehicle speed.

The moment about the x-axis:

$$M_{gx} = I_{wy}\frac{V}{R_0}\dot{\psi}_w. \tag{24}$$

The moment about the z-axis:

$$M_{gz} = -I_{wy}\frac{V}{R_0}\dot{\phi}_w \tag{25}$$

Since the roll motion of the wheel set is calculated by the lateral motion and the wheel/rail relationship, the roll angular velocity in this study is calculated by the following equation:

$$\dot{\phi}_w = \frac{\dot{y}_w(\lambda_L + \lambda_R)}{2d_0}. \tag{26}$$

3. Effect of wheel set gyroscopic action on linear stability

In order to analyse the effect of wheel set gyroscopic action on linear stability, the linear critical speeds in situations with and without gyroscopic action are calculated. Figure 4 shows the variation of the real part of the instability mode with respect to the vehicle speed. Figure 5 shows the root locus diagram of the instability mode. The instability mode in Figures 4 and 5 is the hunting motion of the railway vehicle, which behaves as the swing and yaw motion of the vehicle parts. According to the description in Section 2.3, when

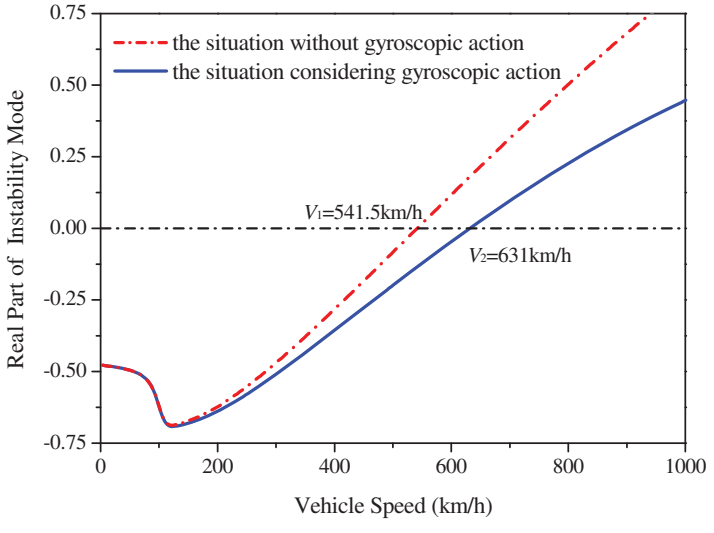

Figure 4. Plot of the real part of the instability mode with respect to speed.

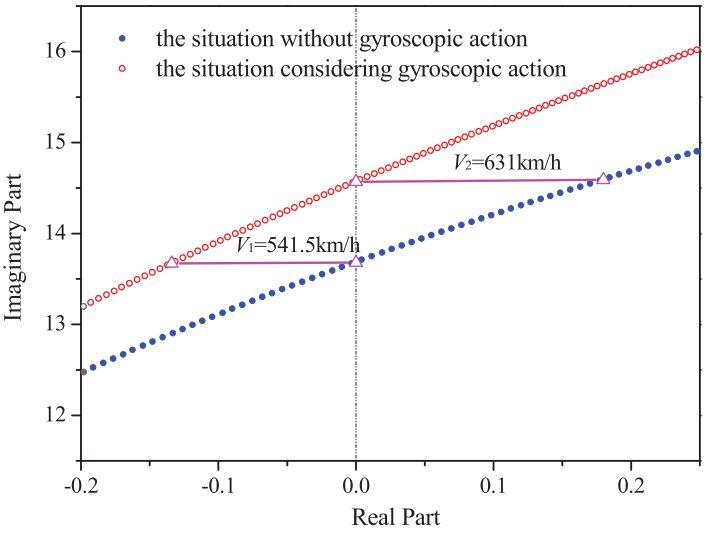

Figure 5. Root locus diagram of the instability mode.

the maximum real part of the eigenvalues of the eigenmatrix in Equation (23) is equal to or greater than zero, the amplitude of hunting motion will not converge to zero. In other words, the mode of hunting motion becomes unstable. To show the root locus briefly and clearly, we plotted only the locus of the eigenvalue corresponding to the mode of hunting motion in Figures 4 and 5. The results in Figures 4 and 5 are obtained on the basis of the nominal design parameters presented in Appendix 2. Figures 4 and 5 show that the linear critical speed is 541.5 km/h in the situation without gyroscopic action, and 631 km/h in the situation considering gyroscopic action. The percentage change is 16.5%. This indicates that the gyroscopic action plays a beneficial role in hunting stability.

It is known from Equations (24) and (25) that the value of the gyroscopic moment is proportional to the vehicle speed. From Figure 4, we can also learn that the gyroscopic

Table 2. Linear critical speeds calculated in the situation with gyroscopic action and the situation without gyroscopic action using different values of primary longitudinal stiffness.

Primary longitudinal stiffness (N/m)	Linear critical speed in the situation without gyroscopic action (km/h)	Linear critical speed in the situation with gyroscopic action (km/h)	Increase of linear critical speed (km/h)	Percentage change
1.096E + 07	730.5	1004.4	273.9	37.50%
1.151E + 07	679.2	882.1	202.9	29.87%
1.206E + 07	636.4	794.6	158.2	24.86%
1.260E + 07	599.7	727.9	128.2	21.38%
1.315E + 07	568.1	674.6	106.5	18.75%
1.370E + 07	541.5	631.1	89.6	16.55%
1.425E + 07	517.8	595.5	77.7	15.01%
1.480E + 07	497.3	565.3	68.0	13.67%
1.534E + 07	478.6	538.8	60.2	12.58%
1.589E + 07	463.0	516.0	53.0	11.45%
1.644E + 07	447.9	496.5	48.6	10.85%

action has little effect at low speeds, i.e. less than 200 km/h, but significant effect at high speeds. In other words, the effect of gyroscopic action on linear stability becomes more and more significant with an increase in vehicle speed.

Further analysis is carried out by comparing the linear critical speeds in situations with and without gyroscopic action, when the suspension parameters are varied. According to our previous study [22], critical speed is sensitive to the primary longitudinal stiffness and the damping of the yaw damper. Hence, the comparison is presented in Tables 2 and 3. To show these data more intuitively, Figures 6 and 7 are plotted according to Tables 2 and 3.

Comparing the situations with and without gyroscopic action, the change and percentage change increases with increasing linear critical speed. This phenomenon is consistent with the results in Figure 4 and Equations (24) and (25).

Table 3. Linear critical speeds calculated in situations with and without gyroscopic action using different damping values of the yaw damper.

Damping of yaw damper (N·s/m)	Linear critical speed in the case without gyroscopic action (km/h)	Linear critical speed in the case with gyroscopic action (km/h)	Change of linear critical speed(km/h)	Percentage change
1.962E + 05	427.4	465.1	37.7	8.82%
2.061E + 05	445.6	489.6	44.0	9.87%
2.159E + 05	466.1	517.8	51.7	11.09%
2.257E + 05	488.7	550.5	61.8	12.65%
2.355E + 05	513.5	588.4	74.9	14.59%
2.453E + 05	541.5	631.3	89.8	16.58%
2.551E + 05	571.7	682.6	110.9	19.40%
2.649E + 05	606.3	743.9	137.6	22.70%
2.747E + 05	644.2	818.7	174.5	27.09%
2.845E + 05	685.8	911.7	225.9	32.94%
2.944E + 05	732.4	1035.6	303.2	41.40%

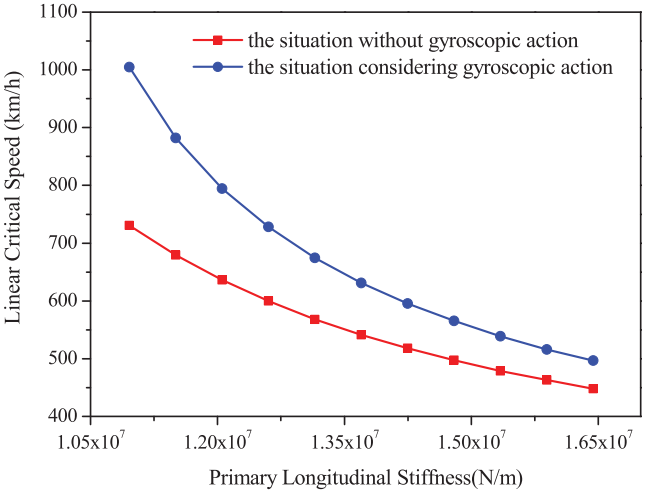

Figure 6. Linear critical speeds calculated in situations with and without gyroscopic action using different values of primary longitudinal stiffness.

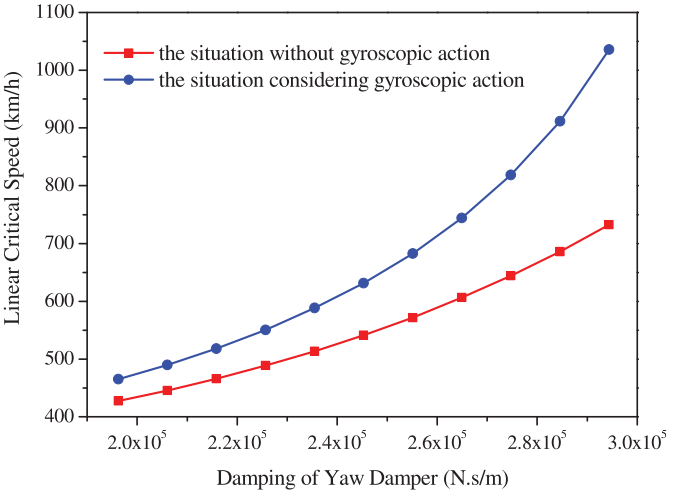

Figure 7. Linear critical speeds calculated in situations with and without gyroscopic action using different damping values of the yaw damper.

4. Effect of wheel set gyroscopic action on nonlinear stability

In this section, the effect of wheel set gyroscopic action on nonlinear stability is studied. We conduct the study by plotting bifurcation diagrams in situations with and without gyroscopic action.

The bifurcation diagram, which is calculated by nominal design parameters related to the lateral motion of the first wheel set in the two situations, is shown in Figure 8. The bifurcation diagram of the dynamical system is a subcritical bifurcation, and there are two non-zero branches (or stable periodic solutions) and a zero branch (or stationary solution).

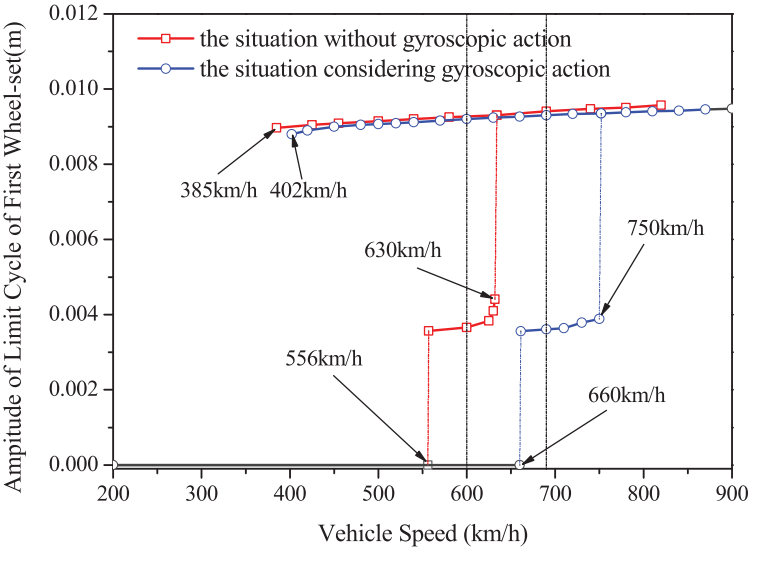

Figure 8. Bifurcation diagram of the lateral motion of the first wheel set.

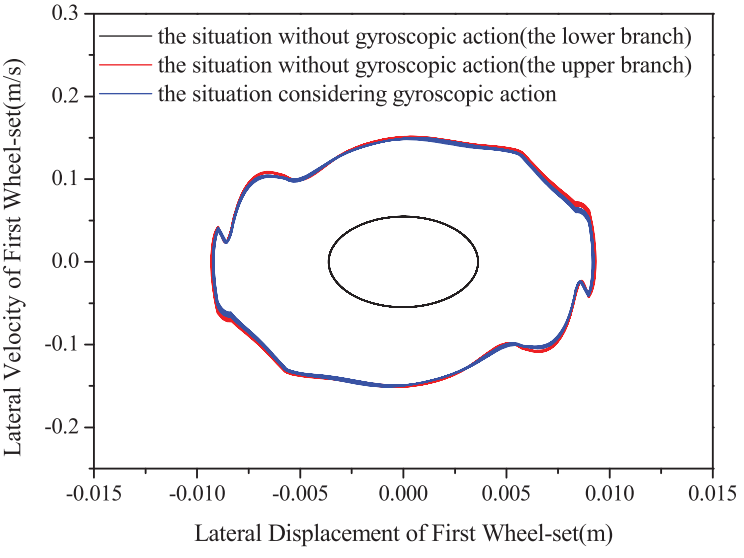

Figure 9. Phase portraits at 600 km/h.

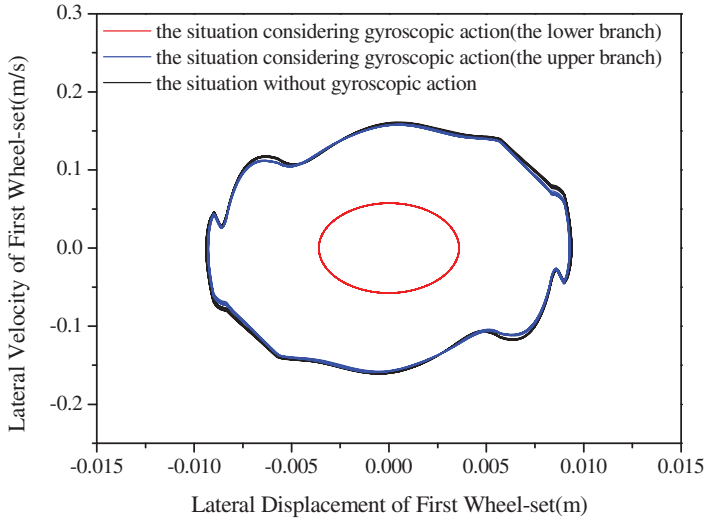

Figure 10. Phase portraits at 690 km/h.

The phase portraits at 600 km/h and 690 km/h are plotted in Figures 9 and 10. The results in Figures 8–10 indicate that the bifurcation characteristics change significantly because of wheel set gyroscopic action.

As shown in Figure 8, compared to the situation without wheel set gyroscopic action, the Hopf bifurcation speed increases from 556 to 660 km/h when the wheel set gyroscopic action is taken into account. The percentage change is 18.7%. Similarly, the nonlinear critical speed increases from 385 to 402 km/h, and the percentage change is 4.4%. If there was no wheel set gyroscopic action, the speed interval of the lower branch would be 556–632 km/h. However, due to the wheel set gyroscopic action, the speed interval of

the lower branch becomes 660–750 km/h. The extension of the speed interval means an improvement of hunting stability.

Assuming that the gyroscopic action does not exist in the speed interval 556–630 km/h, the vehicle will incur a stable periodic motion of small amplitude (the lower branch in the bifurcation diagram) when the vehicle suffers a small disturbance, and incurs a stable periodic motion of large amplitude (the upper branch in the bifurcation diagram) when the vehicle suffers a large disturbance. However, regardless of whether the disturbance is small or not, the vehicle will incur a stable periodic motion of large amplitude in the speed interval 630–660 km/h. In practice, the motion caused by disturbances will decay and converge to the stationary solution in the two speed intervals mentioned above due to wheel set gyroscopic action.

When the vehicle speed exceeds 660 km/h, in the absence of gyroscopic action, the motion undergoing any disturbance would be a stable periodic motion of large amplitude. However, owing to the existence of wheel set gyroscopic action, only a large disturbance can result in a stable periodic motion of large amplitude.

Though the nonlinear critical speed, the Hopf bifurcation speed, and the speed interval of the lower branch are much different between cases with and without gyroscopic action, the amplitudes of the stable periodic solutions in these two cases are quite close. The influence of wheel set gyroscopic action on the amplitude in the stable periodic solutions is limited.

A further analysis is carried out by calculating the variation of the nonlinear critical speeds and the Hopf bifurcation speeds with respect to the primary longitudinal stiffness and the damping of the yaw damper. The nonlinear critical speeds as these two parameters change are shown in Tables 4 and 5. The nonlinear critical speeds and Hopf speeds in situations with gyroscopic action are always greater than in situations without gyroscopic action. This effect on hunting stability is unaffected by changes in suspension parameters.

Table 4. Nonlinear critical speeds and Hopf speeds calculated in situations with and without gyroscopic action using different values of primary longitudinal stiffness.

Parameter: Primary longitudinal stiffness						
	1.315E + 07		1.370E + 07		1.425E + 07	
Value(N/m)	v_b (km/h)	v_n (km/h)	v_b (km/h)	v_n (km/h)	v_b (km/h)	v_n (km/h)
With gyroscopic action	709	379	660	402	619	390
Without gyroscopic action	603	366	556	385	542	353

Table 5. Nonlinear critical speeds and Hopf speeds calculated in situations with and without gyroscopic action using different damping values of the yaw damper.

Parameter 2: Damping of yaw damper						
	2.355E + 05		2.453E + 05		2.551E + 05	
Value(N·s/m)	v_b (km/h)	v_n (km/h)	v_b (km/h)	v_n (km/h)	v_b (km/h)	v_n (km/h)
With gyroscopic action	606	380	660	402	727	388
Without gyroscopic action	533	368	556	385	611	375

5. Comparison of the gyroscopic moments about the *x*- and *z*-axes

The effects of the two kinds of gyroscopic moments shown in Equations (24) and (25) are different. The gyroscopic moment about the *z*-axis works on the yaw motion of the wheel set, as shown in Equation (2). It is known from Equation (25) that the gyroscopic moment is proportional to the roll angular velocity of the wheel set; hence, it can be regarded as a damping moment. When this moment is considered, an extra positive damping term is attached to the vehicle dynamical system.

The moment about the *x*-axis works on the roll motion of the wheel set. However, as mentioned in Section 2.1, the roll and vertical motions of the wheel set are not independent, but determined by the wheel/rail geometrical relationship and the lateral motion of the wheel set. The differential equations of roll and vertical motions of the wheel set are used in this study to derive normal contact forces between the wheel and rail. As a consequence, the effect of moments about the *x*-axis can be regarded as the effect on normal contact forces, as shown in Equation (15).

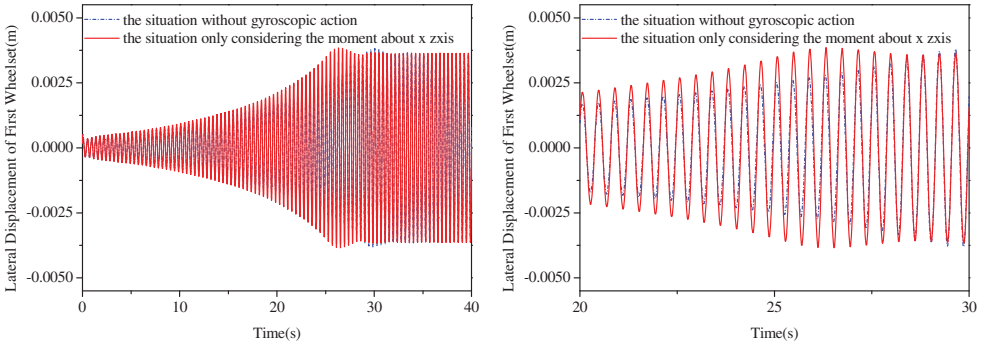

Figure 11. Time history in the situation considering only the moment about the *x*-axis and the situation without gyroscopic action at 600 km/h.

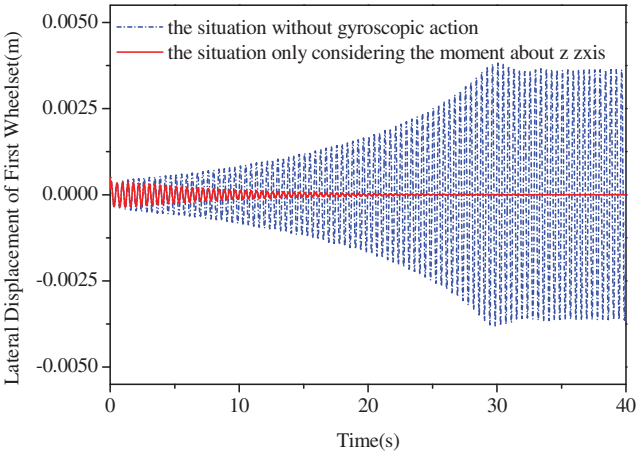

Figure 12. Comparison of the lateral motion of the first wheel set at 600 km/h.

Based on the above analysis, it can be concluded that the effect of gyroscopic action on hunting stability is mainly reflected in yaw motion and normal contact forces. The effects of these two gyroscopic moments are compared in this section. For this comparison, the time histories of 600 km/h in two situations (considering only the moment about the *x*-axis,

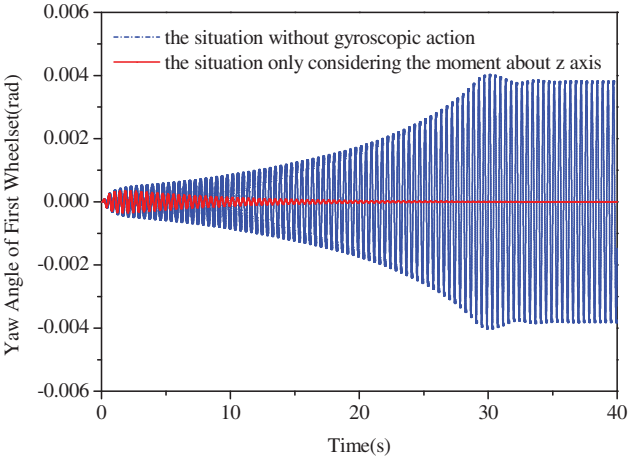

Figure 13. Comparison of the yaw motion of the first wheel set at 600 km/h.

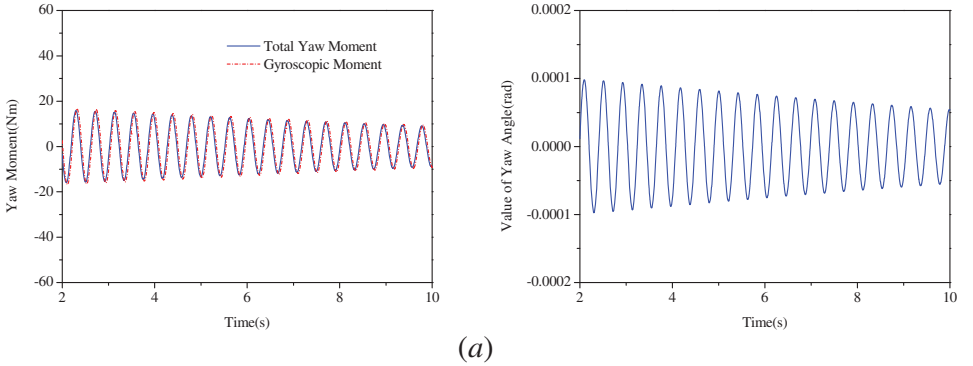

(*a*)

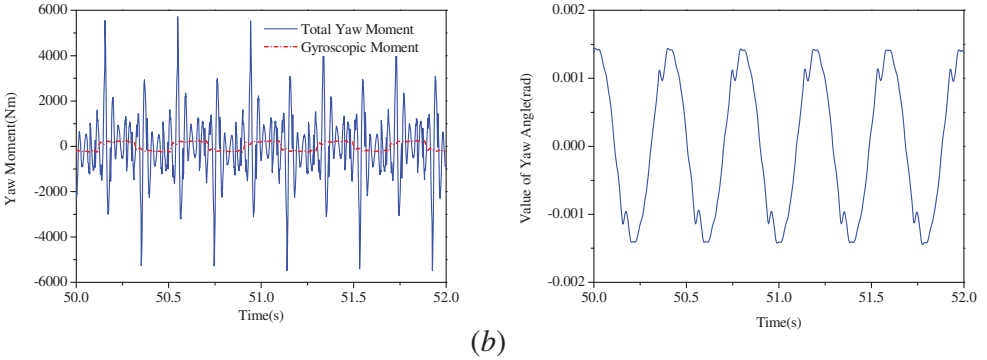

(*b*)

Figure 14. Time history of the moment about the *z*-axis and total yaw moment of the first wheel set at 600 km/h: (a) the motion converges to zero; (b) periodic motion.

and considering only the moment about the z-axis) are calculated. Comparisons with the situation without gyroscopic action are presented below.

Figure 11 shows a comparison between the situation considering only the moment about the x-axis and the situation without gyroscopic action. It is seen from Figure 11 that the wheel set vibration amplitude considering only the moment about the x-axis is slightly larger, and evolves to a limit cycle faster. In other words, the moment about the x-axis is a negative factor for hunting stability.

The comparison between the situation considering only moment about the z-axis and the situation without gyroscopic action is presented in Figures 12 and 13. The results in Figures 12 and 13 show that the wheel set motion converges to zero in the situation considering only the moment about the z-axis, and evolves to a limit cycle if gyroscopic action is not considered. Figures 12 and 13 indicate that the moment about the z-axis is a beneficial factor for hunting stability.

Comparing the results in Figure 11 with the results in Figures 12 and 13, it can be concluded that the effect of the moment about the z-axis is much more significant than the effect of the moment about the x-axis.

To better understand the effect, the moment about the z-axis has in improving the hunting stability, Figure 14 shows the time history of the wheel set yaw moment and the gyroscopic moment about the z-axis, which is obtained in two states of motion (stable periodic solutions and stationary solutions, as shown in Figure 8) at 600 km/h. Figure 15 shows the results obtained in these two states of motion at 690 km/h.

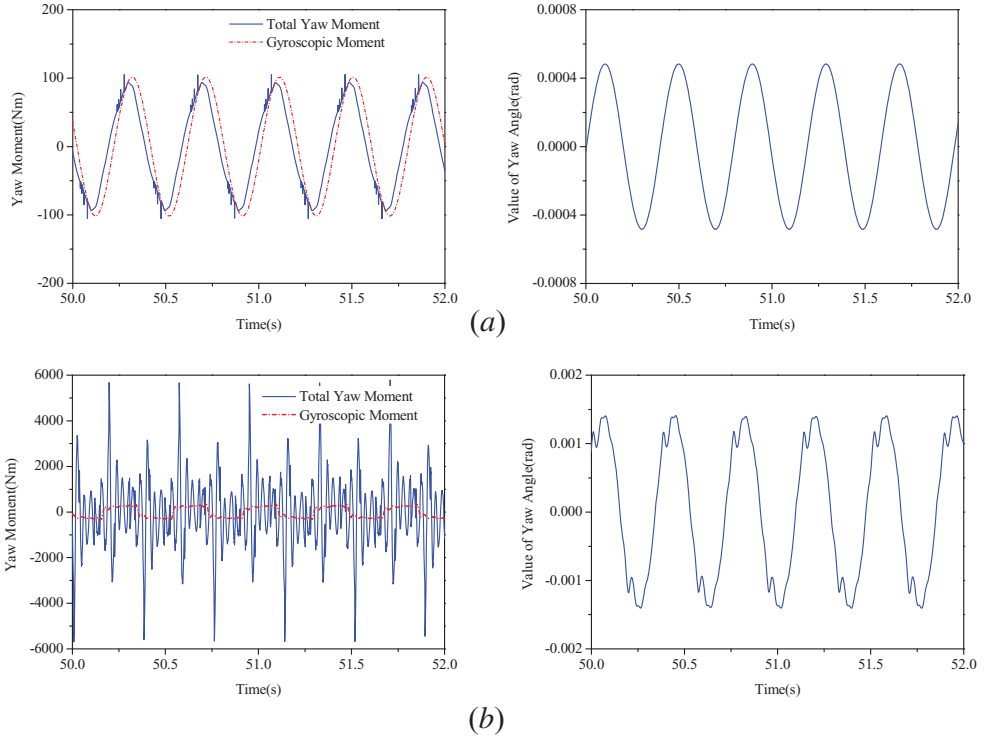

Figure 15. Time history of the moment about the z-axis and total yaw moment of the first wheel set at 690 km/h: (a) periodic motion of small amplitude; (b) periodic motion of large amplitude.

When the vehicle motion is evolving to a stationary solution or a stable periodic solution of small amplitude, the moment about the z-axis is close to the total yaw moment. When the vehicle motion is a stable periodic solution of large amplitude, the frequency and amplitude of the total yaw moment are both larger than those of the moment about the z-axis. However, the amplitudes are of the same magnitude. The results in Figures 14 and 15 also show that there is a 190° phase difference between the dominant vibration of gyroscopic moment and the dominant vibration of yaw angle. This phase difference indicates the inhibiting effect of gyroscopic moment on the wheel set yaw motion.

6. Conclusions

In this study, the effects of wheel set gyroscopic action on linear and nonlinear hunting stability were investigated. To this end, a dynamic model for a high-speed vehicle with 23 DOF was developed by considering wheel set gyroscopic action. The influence of wheel set gyroscopic action on the hunting stability was analysed. Root locus for a linear model and a bifurcation diagram for a nonlinear model in situations with and without gyroscopic action were plotted. Additionally, the effects of the gyroscopic moment about the x-axis and the gyroscopic moment about the z-axis were compared.

The mechanism analysis shows that the effects of wheel set gyroscopic action originate from two kinds of gyroscopic moments. The effects of these two kinds of gyroscopic moments are different. The moment about the z-axis can be considered as an extra damping term attached to the vehicle dynamical system; it is a beneficial factor for hunting stability. The effect of the moment about the x-axis reflects in normal contact forces; it is detrimental to the hunting stability. The simulation of time history indicates that the effect of the moment about the z-axis is much more significant than the effect of the moment about the x-axis. The integrated effect of wheel set gyroscopic action can enhance the critical speeds and suppress the amplitude of periodic motion; it is a beneficial factor for hunting stability. The simulation finds the effect to be small at low vehicle speeds, and becomes larger as the vehicle speed increases.

On the basis of the nominal design parameters of an actual high-speed railway vehicle, the quantitative result of the effect of wheel set gyroscopic action is obtained. Compared to the situation without wheel set gyroscopic action, the linear critical speed increases from 541.5 to 631 km/h, and the nonlinear critical speed and the Hopf bifurcation speed increase from 385 and 556 km/h to 402 and 631 km/h, respectively, when the wheel set gyroscopic action is taken into account. When the designed parameters are changed, the critical speed may be different; however, the effect of wheel set gyroscopic action on hunting stability does not change.

Disclosure Statement

No potential conflict of interest was reported by the authors.

Funding

The project was supported by the National Natural Science Foundation of China (Nos. 11672306, 51490673), the Strategic Priority Research Program of the Chinese Academy of Sciences

(No. XDB22020101), and the National Basic Research Program (973 Program) of China (No. 2014CB046801).

References

[1] Kim P, Jung J, Seok J. A parametric dynamic study on hunting stability of full dual-bogie railway vehicle. Int J Precis Eng Manuf. 2011;12(3):505–519.
[2] Lee SY, Cheng YC. Hunting stability analysis of high-speed railway vehicle trucks on tangent tracks. J Sound Vib. 2005;282(3):881–898.
[3] Lee SY, Cheng YC. Nonlinear analysis on hunting stability for high-speed railway vehicle trucks on curved tracks. J Vib Acoust. 2005;127(4):324–332.
[4] Cheng YC, Lee SY. Stability analysis of high-speed railway vehicle using half-car model. Int J Heavy Veh Syst. 2010;17(2):139–158.
[5] Cheng YC. Hunting stability analysis of a railway vehicle system using a novel non-linear creep model. Proc Instit Mech Eng, Part F: J Rail Rapid Transit. 2012;226(6):612–629.
[6] Cheng YC, Hsu CT. Hunting stability and derailment analysis of a car model of a railway vehicle system. Proc Instit Mech Eng, Part F: J Rail Rapid Transit. 2012;226(2):187–202.
[7] Allen PD, Iwnicki SD. The critical speed of a railway vehicle on a roller rig. Proc Instit Mech Eng, Part F: J Rail Rapid Transit. 2001;215(2):55–64.
[8] True H. Does a critical speed for railroad vehicles exist? In: Railroad conference, 1994, proceedings of the 1994 ASME/IEEE joint (in conjunction with area 1994 annual technical conference). Chicago, IL: IEEE; 1994. p. 125–131.
[9] True H. Multiple attractors and critical parameters and how to find them numerically: the right, the wrong and the gambling way. Veh Syst Dyn. 2013;51(3):443–459.
[10] True H. On the theory of nonlinear dynamics and its applications in vehicle systems dynamics. Veh Syst Dyn. 1999;31(5–6):393–421.
[11] True H, Kaas-Petersen C. A bifurcation analysis of nonlinear oscillations in railway vehicles. Veh Syst Dyn. 1983;12(1–3):5–6.
[12] Kim P, Seok J. Bifurcation analysis on the hunting behaviour of a dual-bogie railway vehicle using the method of multiple scales. J Sound Vib. 2010;329:4017–4039.
[13] Polach O, Kaiser I. Comparison of methods analysing bifurcation and hunting of complex rail vehicle models. J Comput Nonlinear Dyn. 2012;7(4):041005-1–041005-8.
[14] True H. Railway vehicle chaos and asymmetric hunting. Veh Syst Dyn. 1992;20:625–637.
[15] Jensen JC, True H. Chaos and asymmetry in railway vehicle dynamics. Transp Eng. 1994;22:55–68.
[16] True H, Jensen JC. Parameter study of hunting and chaos in railway vehicle dynamics. Veh Syst Dyn. 1994;23:508–521.
[17] Sedighi HM, Shirazi KH. Bifurcation analysis in hunting dynamical behaviour in a railway bogie: using novel exact equivalent functions for discontinuous nonlinearities. Scientia Iranica. 2012;19(6):1493–1501.
[18] Eom BG, Kang BB, Lee HS. A study on running stability assessment methods for 1/5 small scaled bogie of Saemaul using small-scaled derailment simulator. Int J Precis Eng Manuf. 2013;14(4):589–598.
[19] Dong H, Zeng J, Xie JH, et al. Bifurcation\instability forms of high speed railway vehicles. Sci China Technol Sci. 2013;56(7):1685–1696.
[20] Huang CH, Zeng J, Liang SL. Carbody hunting investigation of a high speed passenger car. J Mech Sci Technol. 2013;27(8):2283–2292.
[21] Zeng X, Wu H, Lai J, et al. Hunting stability of high-speed railway vehicles on a curved track considering the effects of steady aerodynamic loads. J Vib Control. 2016;22(20):4159–4175.
[22] Zeng XH, Wu H, Lai J, et al. Influences of aerodynamic loads on hunting stability of high-speed railway vehicles and parameter studies. Acta Mech Sin. 2014;30(6):889–900.
[23] Zboinski K, Dusza M. Development of the method and analysis for non-linear lateral stability of railway vehicles in a curved track. Veh Syst Dyn. 2006;44(sup1):147–157.

[24] Zboinski K, Dusza M. Bifurcation approach to the influence of rolling radius modelling and rail inclination on the stability of railway vehicles in a curved track. Veh Syst Dyn. 2008;46(sup1):1023–1037.
[25] Zboinski K, Dusza M. Self-exciting vibrations and Hopf's bifurcation in non-linear stability analysis of rail vehicles in a curved track. Eur J Mech – A/Solids. 2010;29(2):190–203.
[26] Zboinski K, Dusza M. Extended study of railway vehicle lateral stability in a curved track. Veh Syst Dyn. 2011;49(5):789–810.
[27] Zeng J, Wu P. Stability analysis of high speed railway vehicles. JSME Int J Ser C Mech Syst, Mach Elem Manuf. 2004;47(2):464–470.
[28] Hirotsu T. Simulation of hunting of rail vehicles (4th report, influence of gyroscopic action of wheelsets and spin creepage). Japan Soc Mech Eng (C). 1994;60(572):1244–1250.
[29] Huang SK. The mechanism research on wheelset stability. Southwest Jiaotong University; 2013 (in Chinese).
[30] Kalker JJ. The computation of three-dimensional rolling contact with dry friction. International J Numer Methods Eng. 1979;14(9):1293–1307.
[31] Kalker JJ. Survey of wheel-rail rolling contact theory. Veh Syst Dyn. 1979;8(4):317–358.
[32] Shen ZY, Hedrick JK, Elkins JA. A comparison of alternative creep force models for rail vehicle dynamic analysis. Veh Syst Dyn. 1983;12(1–3):79–83.
[33] Iwnicki S. Handbook of railway vehicle dynamics. London: CRC Press; 2006.

Appendix 1. Explanation of parameters

m_w	Mass of wheel set	h_{tk}	Height of secondary suspension above centre of gravity of bogie
m_t	Mass of bogie	h_{ck}	Vertical distance from secondary suspension to centre of gravity of car body
m_c	Mass of car body	l_c	Half of longitudinal distance of secondary suspension
I_{wx}	Roll moment of inertia of wheel set	k_{ty2}	Stiffness of spring–damping connecting point of lateral damper
I_{tx}	Roll moment of inertia of bogie	c_{ty2}	Damping of spring–damping connecting point of lateral damper
I_{cx}	Roll moment of inertia of car body	h_{th}	Height of lateral damper above centre of gravity of bogie
I_{wy}	Pitch moment of inertia of wheel set	h_{ch}	Vertical distance from lateral damper to centre of gravity of car body
I_{ty}	Pitch moment of inertia of bogie	k_{sx}	Stiffness of spring–damping connecting point of yaw damper
I_{cy}	Pitch moment of inertia of car body	c_{sx}	Damping of spring–damping connecting point of yaw damper
I_{wz}	Yaw moment of inertia of wheel set	d_{sx}	Half of lateral distance of yaw damper
I_{tz}	Yaw moment of inertia of bogie	h_{ts}	Height of yaw damper above centre of gravity of bogie
I_{cz}	Yaw moment of inertia of car body	h_{cs}	Vertical distance from yaw damper to centre of gravity of car body
k_{px}	Longitudinal stiffness of primary suspension	N_L	Left normal contact force
k_{py}	Lateral stiffness of primary suspension	N_R	Right normal contact force
k_{pz}	Vertical stiffness of primary suspension	λ_L	Left contact angle
c_{pz}	Primary vertical damping	λ_R	Right contact angle
d_0	Half of track gauge	F_{yL}	Left lateral creep forces
d_{zx}	Half of lateral distance of primary suspension	F_{yR}	Right lateral creep forces
l_t	Half of longitudinal distance of primary suspension	F_{xL}	Left longitudinal creep forces
h_{tz}	Vertical distance from primary suspension to centre of gravity of bogie	F_{xR}	Right longitudinal creep forces
k_{tx1}	Longitudinal stiffness of secondary suspension	M_z	Creep moment
k_{ty1}	Lateral stiffness of secondary suspension	R_0	Normal wheel radius
k_{tz1}	Vertical stiffness of secondary suspension	W	Axle weight
d_{kh}	Half of lateral distance of secondary suspension		

Appendix 2. Nominal design parameters

Parameters	Value
Mass of wheel set	$m_w = 1780\,\text{kg}$
Mass of bogie	$m_t = 3300\,\text{kg}$
Mass of car body	$m_c = 31374\,\text{kg}$
Roll moment of inertia of wheel set	$I_{wx} = 967\,\text{kg}\cdot m^2$
Roll moment of inertia of bogie	$I_{tx} = 2673\,\text{kg}\cdot m^2$
Roll moment of inertia of car body	$I_{cx} = 120,800\,\text{kg}\cdot m^2$
Pitch moment of inertia of wheel set	$I_{wy} = 118\,\text{kg}\cdot m^2$
Pitch moment of inertia of bogie	$I_{ty} = 1807\,\text{kg}\cdot m^2$
Pitch moment of inertia of car body	$I_{cy} = 1,555,000\,\text{kg}\cdot m^2$
Yaw moment of inertia of wheel set	$I_{wz} = 967\,\text{kg}\cdot m^2$
Yaw moment of inertia of bogie	$I_{tz} = 3300\,\text{kg}\cdot m^2$
Yaw moment of inertia of car body	$I_{cz} = 1,467,400\,\text{kg}\cdot m^2$
Longitudinal stiffness of primary suspension	$k_{px} = 1.37 \times 10^7\,\text{N/m}$
Lateral stiffness of primary suspension	$k_{py} = 5.49 \times 10^6\,\text{N/m}$
Vertical stiffness of primary suspension	$k_{pz} = 1.176 \times 10^6\,\text{N/m}$
Primary vertical damping	$c_{pz} = 19,600\,\text{Ns/m}$
Half of track gauge	$d_0 = 0.7465\,\text{m}$
Half of lateral distance of primary suspension	$d_{zx} = 1.0\,\text{m}$
Half of longitudinal distance of primary suspension	$l_t = 0.75\,\text{m}$
Vertical distance from primary suspension to centre of gravity of bogie	$h_{tz} = 0.064\,\text{m}$
Longitudinal stiffness of secondary suspension	$k_{tx1} = 1.597 \times 10^6\,\text{N/m}$
Lateral stiffness of secondary suspension	$k_{ty1} = 1.597 \times 10^6\,\text{N/m}$
Vertical stiffness of secondary suspension	$k_{tz1} = 9.9 \times 10^5\,\text{N/m}$
Half of lateral distance of secondary suspension	$d_{kh} = 1.23\,m$
Height of secondary suspension above centre of gravity of bogie	$h_{tk} = 0.39\,\text{m}$
Vertical distance from secondary suspension to centre of gravity of car body	$h_{ck} = 0.62\,\text{m}$
Half of longitudinal distance of secondary suspension	$l_c = 8.75\,\text{m}$
Stiffness of spring–damping connecting point of lateral damper	$k_{ty2} = 3.43 \times 10^7\,\text{N/m}$
Damping of spring–damping connecting point of lateral damper	$c_{ty2} = 1.176 \times 10^5\,\text{Ns/m}$
Height of lateral damper above centre of gravity of bogie	$h_{th} = 0.281\,\text{m}$
Vertical distance from lateral damper to centre of gravity of car body	$h_{ch} = 0.719\,\text{m}$
Stiffness of spring–damping connecting point of yaw damper	$k_{sx} = 8.82 \times 10^6\,\text{N/m}$
Damping of spring–damping connecting point of yaw damper	$c_{sx} = 2.89 \times 10^5\,\text{Ns/m}$
Half of lateral distance of yaw damper	$d_{sx} = 1.35$
Height of yaw damper above centre of gravity of bogie	$h_{ts} = -0.03\,\text{m}$
Vertical distance from yaw damper to centre of gravity of car body	$h_{cs} = 1.04\,\text{m}$
Normal wheel radius	$R_0 = 0.43\,\text{m}$
Axle weight	$W = 1.1 \times 10^5\,\text{N}$